Functional behaviour of TiO_2 films doped with noble metals

M.S. Rodrigues[1,2 *], J. Borges[1,3], C. Gabor[4], D. Munteanu[4], M. Apreutesei[5], P. Steyer[5], C. Lopes[1,2], P. Pedrosa[1,3,6], E. Alves[7], N.P. Barradas[8], L. Cunha[1], D. Martínez-Martínez[1], F. Vaz[1,3]

[1]Centro/Dep. de Física, Universidade do Minho, Gualtar, 4710 - 057 Braga, Portugal

[2]Instituto Pedro Nunes, Lab. de Ensaios, Desgaste e Materiais, Rua Pedro Nunes, 3030-199 Coimbra, Portugal

[3]SEG-CEMUC, Mechanical Engineering Dep., Univ. of Coimbra, 3030-788 Coimbra, Portugal

[4]Materials Science Department, Materials Science and Engineering Faculty, Transilvania University of Brasov - Romania, 500036, 29 Eroilor Blvd.

[5]INSA de Lyon, MATEIS Laboratory, Eq. CorrIS/SNMS, Bât. B. Pascal, 7 Av Jean Capelle, 69621-Villeurbanne, France

[6]Universidade do Porto, Faculdade de Engenharia, Departamento de Engenharia Metalúrgica e de Materiais, Rua Dr. Roberto Frias, s/n, 4200-465 Porto, Portugal

[7]Instituto de Plasmas e Fusão Nuclear, Instituto Superior Técnico, Universidade de Lisboa, Av. Rovisco Pais, 1049-001 Lisbon, Portugal

[8]Centro de Ciências e Tecn. Nucleares, Instituto Sup. Técnico, Univ. de Lisboa, E.N. 10 (km 139.7), 2695-066 Bobadela, Portugal

* Corresponding author – mprodrigues@ipn.pt ; marcopsr@gmail.com; +351 966 458 876

Abstract

To evaluate the effects of different concentrations of noble metal in a TiO_2 matrix, different films of both Ag:TiO_2 and Au:TiO_2 systems were prepared. Mechanical and tribological characterization was carried out to evaluate the coatings response as a function of the noble metals composition and (micro)structure of the films. The overall set of results indicates that the amorphous films reveal better results than the crystalline ones. For the amorphous samples, the

reduced Young's modulus and the adhesion critical loads followed similar tendencies in both sets of films. Wear rates were similar for all samples except for the one with the highest silver content. To improve brittleness of TiO_2 films, the results seem to indicate that a slight metal doping is preferred, and Au showed to be a better choice than Ag. In fact, the sample with the lowest Au content revealed a better mechanical behaviour than the pure TiO_2 film.

Keywords: Magnetron sputtering; Thin films; Brittleness; Noble metal doping; Titanium dioxide

Nomenclatures / abbreviations:

χ	Mole %
ν	Poisson ratio
Ag	Silver
Ar	Argon
at.%	Atomic %
Au	Gold
DC	Direct Current
E*	Reduced Young's modulus
ECG	Electrocardiography
EEG	Electroencephalography
EMG	Electromyography
fcc	Face-centered cubic
H	Hardness
LSPR	Localised Surface Plasmon Resonance
n	Number of mole
NPs	nanoparticles
PVD	Physical Vapor Deposition
RBS	Rutherford Backscattering Spectrometry
SEM	Scanning Electron Microscopy
SERS	Surface-Enhanced Raman Spectroscopy
Si	Silicon
TiO_2	Titanium dioxide
XRD	X-Ray Diffraction

1. Introduction

Titanium dioxide (TiO_2) is a transparent semiconductor material, with a high bandgap, varying between 3.0 and 3.4 eV [1-4]. Concerning its behaviour, TiO_2 is known for its biocompatibility, non-toxicity, chemical stability, high hardness and high optical transmittance, combined with a high refractive index, between 2.4 and 2.9 [5-10]. Due to these characteristics, TiO_2 is widely used in

several optical devices, biomedical applications, dye sensitised solar cells, photo-electrolysis, photocatalysis, as a coating for anti-fogging and evn as a self-cleaning coating material for glasses [5, 6, 11]. In basic terms, TiO_2 exists in both amorphous and crystalline forms. Specifically, the two most important crystalline forms are anatase and rutile, both showing a tetragonal-like structure lattice [12]. Among these phases, anatase is known for its excellent photocatalytic activity [12] and it is kinetically stable at low temperatures. In the rutile form, TiO_2 has good structural stability at high temperatures, together with a higher refractive index [13]. On the other way around, in the amorphous form,TiO_2 has high blood compatibility and thus it is often used in several types of biomedical applications [14].

Brittleness is an important feature for any kind of thin films system, which may restrict its use in some applications that require flexible substrates [15-17]. The case of thin film systems designed for polymeric base electrodes or sensors to be used in several types of biomedical applications, including electroencephalography, EEG, and electrocardiography ECG [18] and electromyography, EMG [15, 19, 20], as well as some kinds of biological sensors [21] are particularly noticeable examples, that are being develop in the group for some time. To overcome this drawback and improve flexibility of the coated devices, the tailoring of the elastic modulus [22] of the thin film systems by adding silver (Ag) or gold (Au) to such oxide material, is one of the most promising routines that can be optimized. At the same time, the dispersion of such noble metals (Au, Ag) throughout the TiO_2 matrix can create thin films with metallic nanoparticles (NPs), responsible for the so-called localised surface plasmon resonance (LSPR) [23], which gives rise to a set of unique properties that enables the film system to be used in some appliactions that were fristly impossible when ussing pure oxide-type films.

Furthermore, the absorption bands in the visible spectra range are the main feature associated with the presence of Au and Ag nanoparticles [23]. This effect can produce a palette of colours [9] if one can tune the LSPR position, the bandwidth and peak height through changes on the size, distribution and shape of the NPs, as well as on the host dielectric matrix (such as TiO_2). Consequently, the tailoring of the optical properties of the nanocomposites is possible [24-26].

Beyond colouring that was used for several centuries in the windows of the medieval cathedrals and ancient Roman glass cups, advanced applications of such plasmonic nanocomposite materials include: solar cells, optoelectronic devices, biosensors, gas sensors, magnetic storage, energy conversion, optical filters, photocatalysis and surface-enhanced Raman spectroscopy (SERS) [27-35]. As mentioned before, to overcome the limitation of experimental conditions, LSPR thin films have to be developed with higher robustness and flexibility in order to support mechanical stress. Taking this into account, and in order to evaluate the effects of different concentrations of Au and Ag in a TiO_2 matrix, several thin films of Ag:TiO_2 and Au:TiO_2 systems were produced by reactive magnetron sputtering. This physical vapour deposition technique was chosen since it is known to be an environmentally friendly coating process that provides durable materials with low-cost production, when compared to the traditional preparation methods [42]. The determination of hardness, reduced Young's modulus, wear rate and critical loads [36-38] was performed in order to evaluate the brittleness of the coatings and to correlate the mechanical behaviour with the composition and (micro)structure of the films [17, 39-44].

2. Experimental details

The Au:TiO_2 and Ag:TiO_2 thin films were prepared by reactive DC magnetron sputtering [45], on Si (Boron doped p-type, <100> orientation, thickness of 525 μm), in a custom-made deposition system [45]. The system is composed of a cylindrical deposition chamber (~40 dm^3), a pre-chamber, a vacuum system, a gas flow controller, an electrical system and a control unit. The deposition chamber is composed by two vertically aligned rectangular magnetrons, in a closed field configuration. To produce the films, only one magnetron was used, powered by a Hüttinger PFG 7500 DC (maximum output of 7.5 kW). The primary vacuum of the deposition chamber (with pressures of ~0.3 Pa) is achieved using a rotary vane vacuum pump, a Balzers Duo 012A. The secondary vacuum (with pressures of ~10^{-4} Pa) is obtained using a TurboMolecular vacuum pump, model PTM 5400 (400 L.s−1) from Alcatel. To measure the gas pressure, the system is controlled by a Leybold Penningvac PTR225 (10^{-7}–10 Pa) and a Leybold Sky-Pirani Gauge

TR090 (10^{-2}–10^{5} Pa). The films were prepared using a substrate holder positioned at 70 mm from the target, in a rotation mode-type (9 rpm). A titanium target (200×100×6 mm^3, 99.8% purity) containing different amounts of Au, or Ag, pellets (1 mm thick and 4.5 mm in diameter) incrusted in the erosion track of the Ti target was used. The number of Au or Ag pellets was changed to vary the flux of Au or Ag atoms towards the substrate and thus obtain films with different noble metal concentrations. The power supply connected to the target was set to operate in the current regulating mode, using a current density of 100 $A.m^{-2}$ on the Ti-Au, or Ti-Ag, target. The films were prepared using an atmosphere composed of Ar and O_2 leading to a total pressure of about 4×10^{-1} Pa. To promote and enhance the adhesion of the films, the Si substrates were treated using an *in situ* etching process in Ar (pressure of about 5×10^{-1} Pa) under a pulsed DC current of 0.5 A with a duty cycle of 30%, during 1200 s. Find the etching and deposition parameters summarized in Table 1.

Table 1 – Etching and deposition parameters to produce the coatings

Parameter	Etching	Deposition
Power Source	Pulsed DC Current (T_{on} = 1536 ns, f = 200kHz)	DC Current
Ar (sccm)	70	60
O_2 (sccm)	-	7.5
Time (s)	1200	3600
Current (A/m^2)	25	100
T (ºC)	100	100
Bias	-	Grounded
P_{Work} (Pa)	5×10^{-1}	4×10^{-1}
P_{Base} (Pa)	$\sim10^{-5}$	10^{-5}

The deposition parameters, such as the target potential and current, gas pressure, argon flow and reactive gas flows, were monitored before and during the deposition, using a Data Acquisition/Switch Unit Agilent 34970A, equiped with a multifunction module (334907A), where the cables (from analog outputs

of the power supply, pressure sensors and flow controllers) were connected. This unit uses an RS-232 interface, and the data is acquired with a Benchlink Data Logger III software.

The chemical composition of the films was determined by Rutherford Backscattering Spectrometry (RBS). Measurements were carried out using 2 MeV ^{4}He and 1.4 MeV ^{1}H beams, at normal incidence. Three detectors were employed in the chamber; one located at a 140º scattering angle and two pin-diode detectors located symmetrically to each other, both at a 165º scattering angle respective to the beam direction. The data were analysed with the code NDF [46, 47].

Structural characterization of the coatings was conducted by X-ray diffraction (XRD) in a Bragg-Brentano configuration, in a Brucker D8 Advance diffractometer, operating with a CuKα radiation (λ = 0.154 nm) source. The working voltage of the instrument was 40 kV with a current of 40 mA. The diffraction peaks corresponding to planes <111> and <200> were deconvoluted using the Pearson VII functions to match the peak position, peak intensity and integral breadth, using Winfit software [48, 49]. The grain size was estimated based on the integral breadth method, using the same software. The morphology of the films was analysed by Scanning Electron Microscopy, SEM, in an Ultra-high resolution Field Emission Gun Microscope, NOVA 200 Nano SEM from FEI Company. Secondary electron images were acquired at an acceleration voltage of 10kV.

The scratch tests were performed using a commercial scratch tester from CSM Instruments, equipped with a Rockwell indenter (Steel 100C6) with a tip radius of 100 μm. The scratch length and speed were set to 5 mm and 5 mm/min, respectively. The load was varied between 0.03 N and 3 or 30 N, at a loading rate of 3 N/min or 30 N/min. Figure 1 demonstrates a typical scratch pattern obtained for the films under study. A brittle tensile failure can be seen starting at the arrow LC1 [50, 51], representing the normal load at which the cracking of the film begins. In LC2, one can observe local interfacial spallation, while in LC3 there is a significant interfacial spallation in all track width [52].

The hardness (H) and reduced Young's modulus of the films ($E^* = E/(1-\nu^2)$; where E is the Young's modulus and ν the Poisson ratio) were determined using the Oliver & Pharr Method, from the loading and unloading curves, acquired with a sensing Berkovich nanoindenter from

CSM Instruments (Switzerland), using a maximum load of 60 mN and a maximum depth around 10% of the thickness of the films. The wear rate of the coatings was estimated using a ball-on-disk tribosystem from CSM Instruments (version 4.4.K). The counterpart was an AISI 100Cr6 steel ball of 6 mm diameter. The conditions of the tests were 5 N of applied load, a speed of 5 cm/s, a track diameter of 10 mm and a temperature of 24 ºC and 32% RH. The maximum number of laps (the stop condition) was 1000, and the acquisition rate was 20 Hz. The samples and the balls were cleaned with isopropanol before each wear test. Normalised wear rates were calculated after measurement of the worn track section for each sample, using a Taylor Hobson profilometer.

3. Results and discussion

3.1. Chemical, Morphological and Structural characterisation

RBS analysis revealed an O/Ti atomic ratio very close to 2, suggesting the presence of a roughly stoichiometric TiO_2 matrix. Table 2 summarises the composition and thickness of the representative films, estimated by RBS and cross-section SEM analysis, respectively.

Table 2 – Nobel metal contents and film thickness.

Coating	Noble metal content, (at.%)	Noble metal content, $\chi_{Au,Ag}$ (mole %)	Ti (at.%)	O (at.%)	O/Ti	Thickness (µm)
TiO_2	…	…	34	66	1.9	0.4
Ag14	5	14	32	63	2.0	0.5
Ag46	21	46	25	54	2.1	0.7
Ag63	34	63	20	46	2.3	0.7
Ag72	39	72	15	46	3.1	2.0
Au14	5	14	31	64	2.1	0.3
Au23	9	23	30	61	2.0	0.4
Au43	20	43	26	54	2.1	0.6
Au64	37	64	21	42	2.0	0.6
Au73	46	73	17	37	2.2	0.9

The atomic concentration of silver in the Ag:TiO_2 films varied from 5 to 39 at.%, while the gold concentration in the Au:TiO_2 films, ranged from 5 to 46 at.%. The mole percentage, χ, of noble metal in the film – $n(Au) / (n(Au) + n(TiO_2)) \times 100$ – is also displayed in Table 2. From now on,

the films will be mentioned according to the names used in Table 2 (1st column), corresponding to the noble metal content expressed in mole % ($\chi_{Au,Ag}$).

SEM micrographs displayed in Figure 2(a) show a dense and compact growth for the pure TiO_2 film. The columns can barely be distinguished since they are not very well defined. From this point, both systems follow different tendencies concerning their microstructure when the noble metal (Au or Ag) is added to the TiO_2 growing matrix. With the addition of Ag, the compact structure of TiO_2 is lost, changing to a more porous and disordered one. As it can be observed in Figure 2(b-d), the type of growth is granular-voided in the Ag:TiO_2 films and the surface appears to be very rough, which is an expected behaviour taking into account other related works [15, 53]. In contrast, it is also clear in Figure 2(e-g) that the addition of Au kept the compact and nearly columnar structure of the TiO_2 intact. Only at very high contents of Au ($\chi_{Au} \geq 64$ mol %) the columns seem to disappear, but the film remains dense and smooth, also in agreement with the results found in a recent work [21]. The microstructures of the Ag:TiO_2 samples, observed in Figure 2(b-d), are typical of this system, since the mobility of Ag on TiO_2 is known to be higher than Au [15, 21, 54]. This higher diffusion and aggregation of silver results in the formation of Ag clusters, here demonstrated by the bright spots observed in the corresponding SEM images, Fig. 2.

The XRD patterns of representative samples with different noble metal contents are depicted in Figure 3. Only peaks related to diffraction on Au and Ag phases were detected for some noble metal concentrations, meaning that the TiO_2 matrix remained amorphous. Samples with higher Ag (Figure 3a) and Au (Figure 3b) contents developed a relatively clear crystalline structure. Samples with χ_{Ag} of 63 and 72 mol % (Ag63 and Ag72) showed the typical fcc structure of Ag (ICDD card N° 04-0783) [15, 53]. The crystalline structure is evidenced by the presence of XRD peaks located at 2θ positions of 38.1° and 44.3°, corresponding to <111> and <200> orientations. Therefore, the formation of crystalline silver only occurs above χ_{Ag} of 50 mol %. In the Au:TiO_2 system, Au also starts to crystallise at the highest concentrations ($\chi_{Au} > 50$ mol %), since only the films with χ_{Au} of 64 and 73 mol % (Au64 and Au73), showed the typical fcc structure of gold (ICDD card N° 04-

0784) [28]. In fact, broad peaks corresponding to <111> and <200> planes located at 2θ = 38.2° and 44.4° can clearly be observed.

According to the set of results obtained by XRD one can clearly identify two different regions in both systems: an amorphous zone for lower Ag or Au concentrations (< 50 mol %), where the existing noble atoms/clusters did not aggregate to form crystalline domains, followed by a crystalline zone where the concentration of noble metal in the film is more important. Another important feature that is worth mention is the apparent contradictory results between SEM and XRD. In fact, the sample with a silver content of 14 mol % (sample Ag14) is XRD amorphous, however, small clusters can be screened by SEM, Figure 2. This suggests that the clusters observed in Figure 2(b) are most probably amorphous. These amorphous Ag aggregates have been already reported in other works [55]. With the deconvolution of to XRD peak fitting (using Winfit), the average size of the crystalline silver domains was estimated to be about 18 nm, in the samples with silver contents of 63 and 72 mol % (samples Ag63 and Ag72, respectively). In the case of the two films with the highest Au contents, the grain size was estimated to be below 5 nm, revealing a significant grain size reduction. These results demonstrate, once again, silver aggregate easier into clusters, if compared to gold.

3.2. Mechanical Properties

Figure 4 depicts the hardness (*H*) and reduced Young's modulus (*E**) as a function of the noble metal mol % (χ) in each identified zone (amorphous and crystalline, accordingly with the structural analysis). For the TiO_2 film, the hardness and the reduced Young's modulus showed values of 11 GPa and 166 GPa, respectively, which are in agreement with the values found in several published works [56-58]. From Figure 4 one can observe that for the film with the smallest Au concentrations, the hardness and reduced Young's modulus was higher than the TiO_2 film. However, these values are tendentiously lower when both Au and Ag contents are above 14 mol %, in comparison with the pure host matrix (TiO_2).

The increase of the Au contents led to a gradual decrease of hardness in both amorphous and crystalline zones. From the amorphous to the crystalline zone, the variation of the reduced Young's modulus is not significant for the Au:TiO_2 system. The addition of Ag led to a decrease of the hardness in the amorphous zone, decreasing further when the samples became more crystalline. Concerning the reduced Young's modulus, a small increment was observed in the amorphous zone. However, this parameter decreased sharply on moving to the films indexed to the crystalline zone. This decline in hardness is most likely due to the higher ductility that gold and silver are introducing in the doped TiO_2 coating [58], demonstrating an important feature of this thin films systems if one intends to use them in flexible-like applications such as those mentioned in the biomedical field.

In order to evaluate the flexibility of the coatings [59], the ratio between hardness and reduced Young's modulus, H/E^*, was calculated, and the results are presented in Table 3. In comparison to TiO_2, one can report that the ratio H/E^* is approaching 0.1 in the films with gold contents of 14, 23 and 43 mol % (samples Au14, Au23 and Au 43, respectively), correpsonding to the films indexed to the amorphous Au:TiO_2 zone. This is again a clear indication of increasing flexibility [59]. Nonetheless, this trend is not observed for the crystalline Au:TiO_2 samples and for the whole series of Ag:TiO_2 films since the H/E^* values are decreasing in comparison to TiO_2 film.

Table 3 – Hardness of the films and the ratio between hardness and reduced Young's modulus

Coating	**H (GPa)**	**H/E* ($\times 10^{-2}$)**
TiO_2	11	6.6
Ag14	7.2	5.1
Ag46	3.3	2.2
Ag63	3.7	3.9
Ag72	1.4	2.3
Au14	13.1	7.2
Au23	10.8	7.3
Au43	10.3	7.0
Au64	8.3	5.2
Au73	6.1	4.1

The cohesion of the films and their adhesion to the substrates are also essential for the needed functionalities. Figure 5 displays the critical loads as a function of the noble metal mol %. All three critical loads (LC1, LC2 and LC3) have similar tendencies in both systems. Their values increase when a small content of noble metal is added to the pure TiO_2 film (less than 50 mol % of Ag or Au). In the crystalline zone, the critical loads decrease to values even lower than those of the reference critical load values of TiO_2 film.

The wear rate of the samples as a function of Ag or Au content is shown in Figure 6. The plot shows that the best wear behaviour is provided by the samples with lower noble metal concentrations, indexed to the amorphous zone. In the crystalline zone, the addition of Au does not significantly affect the wear rate, always remaining below the TiO_2 film. The wear rate of the Ag:TiO_2 films indexed to the crystalline zone is also relatively low. Nevertheless, the sample with the highest Ag content reveals an increase of one order of magnitude in this tribological parameter. This sample also showed a very low adhesion and the worst mechanical behaviour, probably due to the low shear strength of silver (in higher amounts) that is segregated to the thin film surface [15, 60]. Another plausible explanation for the high wear rate of this sample is that the Ag particles may agglomerate and cause abrasive wear. In fact, as reported in a previous work from C.P. Twist et al. [61], some Ag aggregates might produce a scar in the wear track and thus affecting the wear mechanisms.

4. Conclusions

In order to investigate the influence of Ag or Au doping in the brittleness of a TiO_2 matrix, several thin films of Ag:TiO_2 and Au:TiO_2 were successfully produced by reactive DC magnetron sputtering, using a titanium target and only a few noble metal pellets. The noble metal concentration for the two sets of films, Ag:TiO_2 and Au:TiO_2, ranged from 14 to 72 mol % Ag and from 14 to 73 mol % Au, respectively. The structural and morphological analysis of the films showed significant differences in the structural evolution during film growth. The XRD analysis showed amorphous samples for metal concentrations of Ag (χ_{Ag}) up to 46 mol % and Au (χ_{Au}) up

to 43 mol % and, for higher noble metal concentrations, crystalline phases of Ag ($\chi_{Ag} \geq 63$ mol %) and Au ($\chi_{Au} \geq 64$ mol %) could be detected. While the addition of Au to the growing TiO_2 matrix kept the compact and columnar type of growth almost unchanged, the increase in Ag in the matrix induces the formation of Ag clusters and porous microstructures.

In terms of functional behaviour, the crystalline films have, in general, worse adhesion, mechanical and tribological properties than the amorphous coatings. Comparing the two systems, it was possible to conclude that for similar mol % of noble metal (Ag, Au) the mechanical properties of the Au doped TiO_2 are, in general, better than the Ag doped TiO_2, also confirmed by analysing the ratio H/E^*. Regarding adhesion, the distinction between the two systems is not clear, only the sample with the smallest content of gold exhibits a much higher adhesion. For the wear rates, similar values were obtained, but gold doping is generally better.

A major important result is that the sample with the lower Au content ($\chi_{Au} = 14$ mol %) revealed the best functional performance under the performed tests, being the only one that improved the mechanical properties of the host matrix (TiO_2). Therefore, one can conclude that to improve the brittleness of TiO_2 films, to be used on flexible substrates such as polymeric electrodes and sensors, slight doping is preferred, and Au is preferable than Ag in terms of performance.

Acknowledgements:

This research was sponsored by FEDER funds through the COMPETE program (Programa Operacional Factores de Competitividade) and by FCT (Fundação para a Ciência e a Tecnologia), under the projects PEST-C/FIS/UI607/2013 and PEst-C/EME/UI0285/2013. The authors also acknowledge the financial support by the project Nano4color - – Design and develop a new generation of color PVD coatings for decorative applications (FP7 EC R4SME Project No. 315286)

References

1. S. S. Cetin, S. Corekci, M. Cakmak, and S. Ozcelik: 'Structural investigation and electronic band transitions of nanostructured TiO2 thin films', *Crystal Research and Technology*, 2011, **46**(11), 1207-1214.

2. D. O. Scanlon, C. W. Dunnill, J. Buckeridge, S. A. Shevlin, A. J. Logsdail, S. M. Woodley, C. R. A. Catlow, M. J. Powell, R. G. Palgrave, I. P. Parkin, G. W. Watson, T. W. Keal, P. Sherwood, A. Walsh, and A. A. Sokol: 'Band alignment of rutile and anatase TiO2', *Nature Materials*, 2013, **12**(9), 798-801.
3. B. Prasai, B. Cai, M. K. Underwood, J. P. Lewis, and D. A. Drabold: 'Properties of amorphous and crystalline titanium dioxide from first principles', *Journal of Materials Science*, 2012, **47**(21), 7515-7521.
4. T. Rojviroon and S. Sirivithayapakorn: 'Properties of TiO2 thin films prepared using sol–gel process', *Surface Engineering*, 2013, **29**(1), 77-80.
5. S. H. Kang, M. S. Kang, H. S. Kim, J. Y. Kim, Y. H. Chung, W. H. Smyri, and Y. E. Sung: 'Columnar rutile TiO2 based dye-sensitized solar cells by radio-frequency magnetron sputtering', *Journal of Power Sources*, 2008, **184**(1), 331-335.
6. D. H. Song, S. H. Uhm, S. B. Lee, J. G. Han, and K. N. Kim: 'Antimicrobial silver-containing titanium oxide nanocomposite coatings by a reactive magnetron sputtering', *Thin Solid Films*, 2011, **519**(20), 7079-7085.
7. T. Shibata, H. Irie, and K. Hashimoto: 'Photoinduced hardness change on TiO2 single crystal surfaces', *Chemical Communications*, 2009(25), 3735-3737.
8. J. R. Devore: 'REFRACTIVE INDICES OF RUTILE AND SPHALERITE', *Journal of the Optical Society of America*, 1951, **41**(6), 416-419.
9. M. Torrell, L. Cunha, M. R. Kabir, A. Cavaleiro, M. I. Vasilevskiy, and F. Vaz: 'Nanoscale color control of TiO2 films with embedded Au nanoparticles', *Materials Letters*, 2010, **64**(23), 2624-2626.
10. J. K. Yao, H. L. Huang, J. Y. Ma, Y. X. Jin, Y. A. Zhao, J. D. Shao, H. B. He, K. Yi, Z. X. Fan, F. Zhang, and Z. Y. Wu: 'High refractive index TiO2 film deposited by electron beam evaporation', *Surface Engineering*, 2009, **25**(3), 257-260.
11. H. Lee, Y. K. Park, S. J. Kim, J. H. Park, S. J. Ki, and S. C. Jung: 'TiO2 photocatalyst film using circulating fluidised bed–chemical vapour deposition', *Surface Engineering*, 2015, **31**(2), 134-139.
12. K. Eufinger, E. N. Janssen, H. Poelman, D. Poelman, R. De Gryse, and G. B. Marin: 'The effect of argon pressure on the structural and photocatalytic characteristics of TiO2 thin films deposited by d.c. magnetron sputtering', *Thin Solid Films*, 2006, **515**(2), 425-429.
13. J. G. Yu and X. J. Zhao: 'Effect of substrates on the photocatalytic activity of nanometer TiO2 thin films', *Materials Research Bulletin*, 2000, **35**(8), 1293-1301.
14. B. S. Liu, X. J. Zhao, Q. N. Zhao, C. L. Li, and X. He: 'The effect of O-2 partial pressure on the structure and photocatalytic property of TiO2 films prepared by sputtering', *Materials Chemistry and Physics*, 2005, **90**(1), 207-212.
15. C. Lopes, P. Fonseca, T. Matama, A. Gomes, C. Louro, S. Paiva, and F. Vaz: 'Protective Ag:TiO2 thin films for pressure sensors in orthopedic prosthesis: the importance of composition, structural and morphological features on the biological response of the coatings', *Journal of Materials Science-Materials in Medicine*, 2014, **25**(9), 2069-2081.
16. O. Borrero-Lopez, M. Hoffman, A. Bendavid, and P. J. Martin: 'The use of the scratch test to measure the fracture strength of brittle thin films', *Thin Solid Films*, 2010, **518**(17), 4911-4917.
17. W. G. Zhang, W. M. Liu, and C. T. Wang: 'Tribological behavior of sol-gel TiO2 films on glass', *Wear*, 2002, **253**(3-4), 377-384.
18. P. Pedrosa, C. Lopes, N. Martin, C. Fonseca, and F. Vaz: 'Electrical characterization of Ag:TiN thin films produced by glancing angle deposition', *Materials Letters*, 2014, **115**(0), 136-139.
19. A. Ferreira, C. Lopes, N. Martin, S. Lanceros-Méndez, and F. Vaz: 'Nanostructured functional Ti–Ag electrodes for large deformation sensor applications', *Sensors and Actuators A: Physical*, 2014, **220**(0), 204-212.
20. C. Lopes, C. Gonçalves, P. Pedrosa, F. Macedo, E. Alves, N. P. Barradas, N. Martin, C. Fonseca, and F. Vaz: 'TiAgx thin films for lower limb prosthesis pressure sensors: Effect of composition and structural changes on the electrical and thermal response of the films', *Applied Surface Science*, 2013, **285, Part A**(0), 10-18.
21. J. Borges, T. Kubart, S. Kumar, K. Leifer, M. S. Rodrigues, N. Duarte, B. Martins, J. P. Dias, A. Cavaleiro, and F. Vaz: 'Microstructural evolution of Au/TiO2 nanocomposite films: The influence of Au concentration and thermal annealing', *Thin Solid Films*, 2015, **580**(0), 77-88.

22. M. Kikuchi, M. Takahashi, and O. Okuno: 'Elastic moduli of cast Ti-Au, Ti-Ag, and Ti-Cu alloys', *Dental Materials*, 2006, **22**(7), 641-646.
23. E. Hutter and J. H. Fendler: 'Exploitation of localized surface plasmon resonance', *Advanced Materials*, 2004, **16**(19), 1685-1706.
24. T. C. He, C. S. Wang, X. Pan, and Y. L. Wang: 'Nonlinear optical response of Au and Ag nanoparticles doped polyvinylpyrrolidone thin films', *Physics Letters A*, 2009, **373**(5), 592-595.
25. L. J. Sherry, R. C. Jin, C. A. Mirkin, G. C. Schatz, and R. P. Van Duyne: 'Localized surface plasmon resonance spectroscopy of single silver triangular nanoprisms', *Nano Letters*, 2006, **6**(9), 2060-2065.
26. C. L. Nehl, H. W. Liao, and J. H. Hafner: 'Optical properties of star-shaped gold nanoparticles', *Nano Letters*, 2006, **6**(4), 683-688.
27. G. Walters and I. P. Parkin: 'The incorporation of noble metal nanoparticles into host matrix thin films: synthesis, characterisation and applications', *Journal of Materials Chemistry*, 2009, **19**(5), 574-590.
28. M. Torrell, P. Machado, L. Cunha, N. M. Figueiredo, J. C. Oliveira, C. Louro, and F. Vaz: 'Development of new decorative coatings based on gold nanoparticles dispersed in an amorphous TiO2 dielectric matrix', *Surface and Coatings Technology*, 2010, **204**(9-10), 1569-1575.
29. C. M. Wang, V. Shutthanandan, Y. Zhang, S. Thevuthasan, L. E. Thomas, W. J. Weber, and G. Duscher: 'Atomic level imaging of Au nanocluster dispersed in TiO2 and SrTiO3', *Nuclear Instruments & Methods in Physics Research Section B-Beam Interactions with Materials and Atoms*, 2006, **242**(1-2), 380-382.
30. R. M. Walton, D. J. Dwyer, J. W. Schwank, and J. L. Gland: 'Gas sensing based on surface oxidation reduction of platinum-titania thin films I. Sensing film activation and characterization', *Applied Surface Science*, 1998, **125**(2), 187-198.
31. K. L. Kelly, E. Coronado, L. L. Zhao, and G. C. Schatz: 'The optical properties of metal nanoparticles: The influence of size, shape, and dielectric environment', *Journal of Physical Chemistry B*, 2003, **107**(3), 668-677.
32. P. Alivisatos: 'The use of nanocrystals in biological detection', *Nature Biotechnology*, 2004, **22**(1), 47-52.
33. M. Torrell, L. Cunha, A. Cavaleiro, E. Alves, N. P. Barradas, and F. Vaz: 'Functional and optical properties of Au:TiO2 nanocomposite films: The influence of thermal annealing', *Applied Surface Science*, 2010, **256**(22), 6536-6542.
34. K. J. Xu, W. J. Yang, and S. H. Dong: 'Effect of Ag/N codoping on photoactivity of TiO2 thin film', *Surface Engineering*, 2011, **27**(7), 480-484.
35. M. G. Hosseini, M. M. Momeni, and M. Faraji: 'Preparation and electrocatalytic activity of gold nanoparticle embedded in highly ordered TiO2 nanotube array electrode for electro-oxidation of galactose', *Surface Engineering*, 2011, **27**(10), 784-789.
36. F. Vaz, P. Machado, L. Rebouta, P. Cerqueira, P. Goudeau, J. P. Rivière, E. Alves, K. Pischow, and J. de Rijk: 'Mechanical characterization of reactively magnetron-sputtered TiN films', *Surface and Coatings Technology*, 2003, **174-175**, 375-382.
37. F. Vaz, L. Rebouta, R. M. C. Da Silva, M. F. Da Silva, and J. C. Soares: 'Characterization of titanium silicon nitride films deposited by PVD', *Vacuum*, 1999, **52**(1-2), 209-214.
38. N. C. Raut, N. Kumar, T. Mathews, S. Dash, A. K. Tyagi, and B. Raj: 'Tribological properties of nanostructured TiO2 coatings', *Surface Engineering*, 2012, **28**(3), 182-186.
39. D. Munteanu, C. Gabor, D. G. Constantin, B. Varga, R. Adochite, O. C. Andrei, J. M. Chappé, L. Cunha, C. Moura, and F. Vaz: 'Friction and wear behaviours of Ti(C,O,N) dark decorative coatings', *Tribology International*, 2011, **44**(7-8), 820-828.
40. D. Munteanu, C. Ionescu, C. Olteanu, A. Munteanu, F. Davin, L. Cunha, C. Moura, and F. Vaz: 'Influence of composition and structural properties in the tribological behaviour of magnetron sputtered Ti-Si-C nanostructured thin films, prepared at low temperature', *Wear*, 2010, **268**(3-4), 552-557.
41. F. Vaz, L. Rebouta, S. Ramos, A. Cavaleiro, M. F. da Silva, and J. C. Soares: 'Physical and mechanical properties of Ti1-xSixN films', *Surface & Coatings Technology*, 1998, **100**(1-3), 110-115.

42. D. Munteanu, F. Vaz, C. Lopes, S. Carvalho, A. Veteleanu, B. Borcea, C. Ionescu, and A. Munteanu: 'Researches on the dependence between processing conditions and some tribological properties of Ti-Si-C thin films', *Metalurgia International*, 2008, **13**(2), 51-56.
43. L. Cunha, F. Vaz, C. Moura, D. Munteanu, C. Lonescu, J. P. Rivière, and E. Le Bourhis: 'Ti-Si-C thin films produced by magnetron sputtering: Correlation between physical properties, mechanical properties and tribological behavior', *Journal of Nanoscience and Nanotechnology*, 2010, **10**(4), 2926-2932.
44. C. Olteanu, D. Munteanu, C. Lonescu, A. Munteanu, J. M. Chappé, L. Cunha, and F. Vaz: 'Tribological characterisation of magnetron sputtered Ti(C, O, N) thin films', *International Journal of Materials and Product Technology*, 2010, **39**(1-2), 186-194.
45. J. Borges, N. Martin, N. P. Barradas, E. Alves, D. Eyidi, M. F. Beaufort, J. P. Riviere, F. Vaz, and L. Marques: 'Electrical properties of AlN xO y thin films prepared by reactive magnetron sputtering', *Thin Solid Films*, 2012, **520**(21), 6709-6717.
46. N. P. Barradas, C. Jeynes, and R. P. Webb: 'Simulated annealing analysis of Rutherford backscattering data', *Applied Physics Letters*, 1997, **71**(2), 291-293.
47. N. P. Barradas, C. Jeynes, and M. A. Harry: 'RBS/simulated annealing analysis of iron-cobalt silicides', *Nuclear Instruments & Methods in Physics Research Section B-Beam Interactions with Materials and Atoms*, 1998, **136**, 1163-1167.
48. A. Ruhm, B. P. Toperverg, and H. Dosch: 'Supermatrix approach to polarized neutron reflectivity from arbitrary spin structures', *Physical Review B*, 1999, **60**(23), 16073-16077.
49. J. Borges, C. Fonseca, N. P. Barradas, E. Alves, T. Girardeau, F. Paumier, F. Vaz, and L. Marques: 'Influence of composition, bonding characteristics and microstructure on the electrochemical and optical stability of AlOxNy thin films', *Electrochim. Acta*, 2013, **106**, 23-34.
50. S. J. Bull: 'Failure mode maps in the thin film scratch adhesion test', *Tribology International*, 1997, **30**(7), 491-498.
51. K. Holmberg and A. Matthews: 'Coatings Tribology: Properties, Mechanisms, Techniques and Applications in Surface Engineering'; 2009, Elsevier Science.
52. R. Jacobs, J. Meneve, G. Dyson, D. G. Teer, N. M. Jennett, P. Harris, J. von Stebut, C. Comte, P. Feuchter, A. Cavaleiro, H. Ronkainen, K. Holmberg, U. Beck, G. Reiners, and C. D. Ingelbrecht: 'A certified reference material for the scratch test', *Surface & Coatings Technology*, 2003, **174**, 1008-1013.
53. R. C. Adochite, D. Munteanu, M. Torrell, L. Cunha, E. Alves, N. P. Barradas, A. Cavaleiro, J. P. Riviere, E. Le Bourhis, D. Eyidi, and F. Vaz: 'The influence of annealing treatments on the properties of Ag:TiO 2 nanocomposite films prepared by magnetron sputtering', *Applied Surface Science*, 2012, **258**(8), 4028-4034.
54. J. Kulczyk-Malecka, P. J. Kelly, G. West, G. C. B. Clarke, J. A. Ridealgh, K. P. Almtoft, A. L. Greer, and Z. H. Barber: 'Investigation of silver diffusion in TiO2/Ag/TiO2 coatings', *Acta Materialia*, 2014, **66**(0), 396-404.
55. S. Liu, W. Huang, S. Chen, S. Avivi, and A. Gedanken: 'Synthesis of X-ray amorphous silver nanoparticles by the pulse sonoelectrochemical method', *Journal of Non-Crystalline Solids*, 2001, **283**(1–3), 231-236.
56. A. Haseeb, M. M. Hasan, and H. H. Masjuki: 'Structural and mechanical properties of nanostructured TiO2 thin films deposited by RF sputtering', *Surface & Coatings Technology*, 2010, **205**(2), 338-344.
57. S. S. Pradhan, S. Sahoo, and S. K. Pradhan: 'Influence of annealing temperature on the structural, mechanical and wetting property of TiO2 films deposited by RF magnetron sputtering', *Thin Solid Films*, 2010, **518**(23), 6904-6908.
58. W. M. Liu, Y. X. Chen, G. T. Kou, T. Xu, and D. C. Sun: 'Characterization and mechanical/tribological properties of nano Au-TiO2 composite thin films prepared by a sol-gel process', *Wear*, 2003, **254**(10), 994-1000.
59. J. Musil, J. Sklenka, and J. Prochazka: 'Protective over-layer coating preventing cracking of thin films deposited on flexible substrates', *Surface & Coatings Technology*, 2014, **240**, 275-280.
60. K. Kutschej, C. Mitterer, C. P. Mulligan, and D. Gall: 'High-temperature tribological behavior of Cr ' N-Ag self-lubricating coatings', *Advanced Engineering Materials*, 2006, **8**(11), 1125-1129.

61. C. P. Twist, A. M. Seyam, C. Chen, M.-G. Kim, M. P. Weberski, N. Ren, T. J. Marks, Y.-W. Chung, and Q. J. Wang: 'Molecularly-Engineered Lubricants: Synthesis, Activation, and Tribological Characterization of Silver Complexes as Lubricant Additives', *Advanced Engineering Materials*, 2012, **14**(1-2), 101-105.

Figure captions

Figure 1 – Example of a typical scratch test performed in the films, indicating LC1, LC2 and LC3 according to optical confirmation. The debris at the coating surface as small pieces of the film that were removed as a consequence of the tip scratch in the coating surface.

Figure 2 - SEM cross-section micrographs of (a) TiO_2 ; (b – d) Ag:TiO_2 and (e – g) Au:TiO_2 films.

Figure 3 - XRD diffractograms of (a) Au:TiO_2 and (b) Ag:TiO_2.

Figure 4 – Hardness (a) and reduced Young's modulus (b) of the films as a function of the noble metal mole %.

Figure 5 - Critical Loads (LC1, LC2 and LC3) as a function of the (a) Ag mole % and (b) Au mole %.

Figure 6 - Wear Rate of the films as a function of noble metal mole %.

Table captions

Table 1 – Etching and deposition parameters to produce the coatings

Table 2 – Nobel metal contents and film thickness.

Table 3 – Hardness and reduced Young's modulus ratio

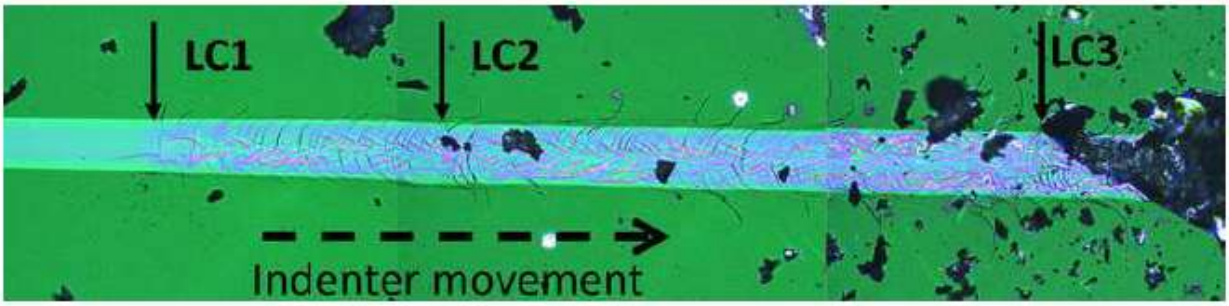

Figure 1

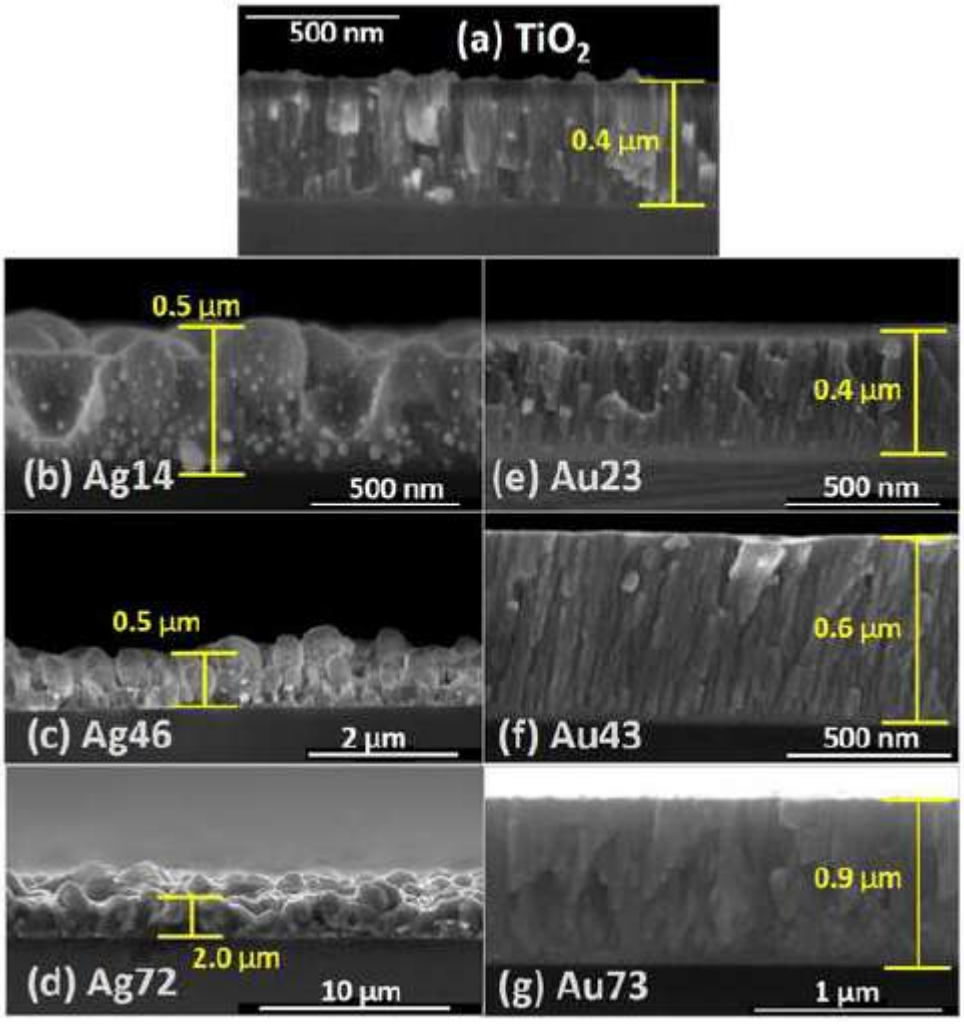

Figure 2

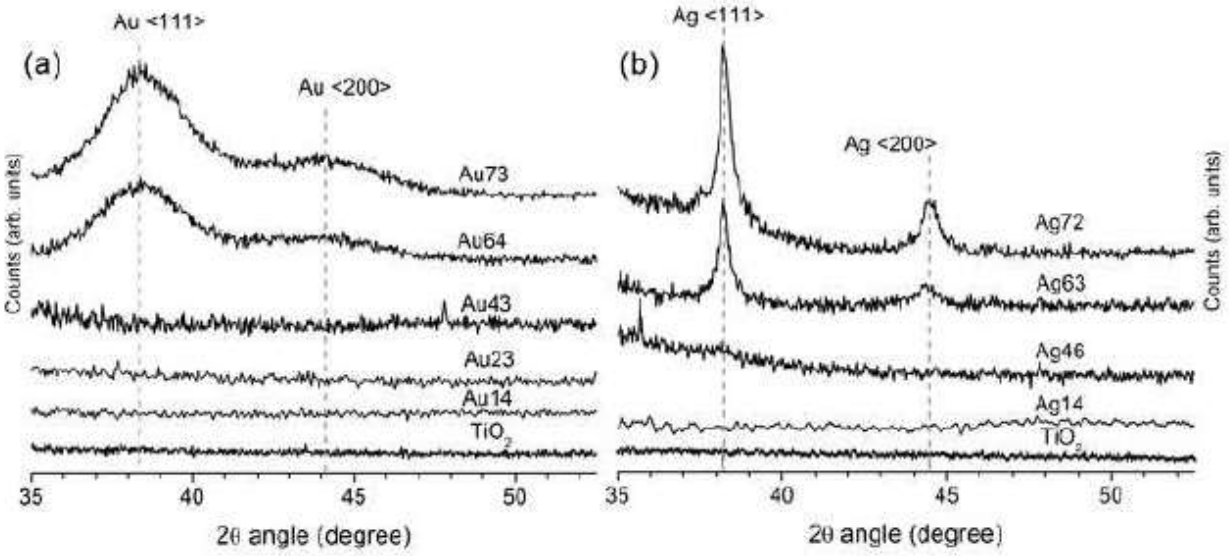

Figure 3

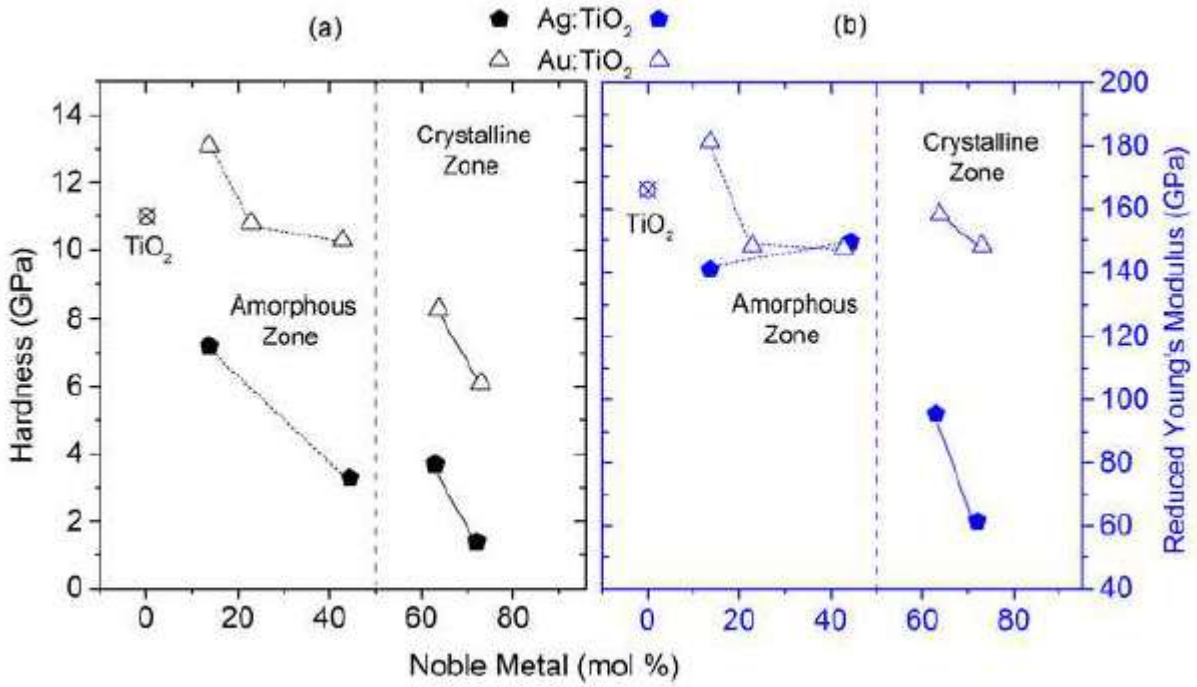

Figure 4

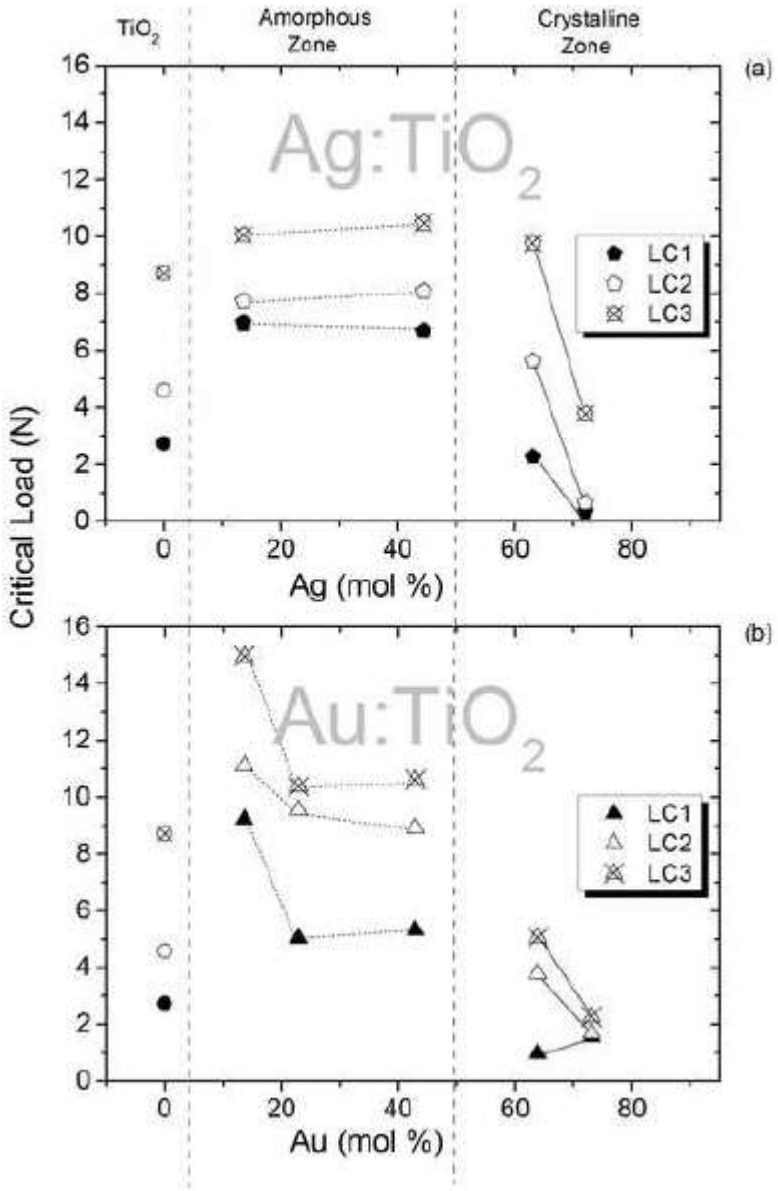
TiO2
Amorphous Zone
Crystaline Zone
(a)
Ag:TiO2
LC1
LC2
LC3
Critical Load (N)
Ag (mol %)
(b)
Au:TiO2
LC1
LC2
LC3
Au (mol %)

Figure 5

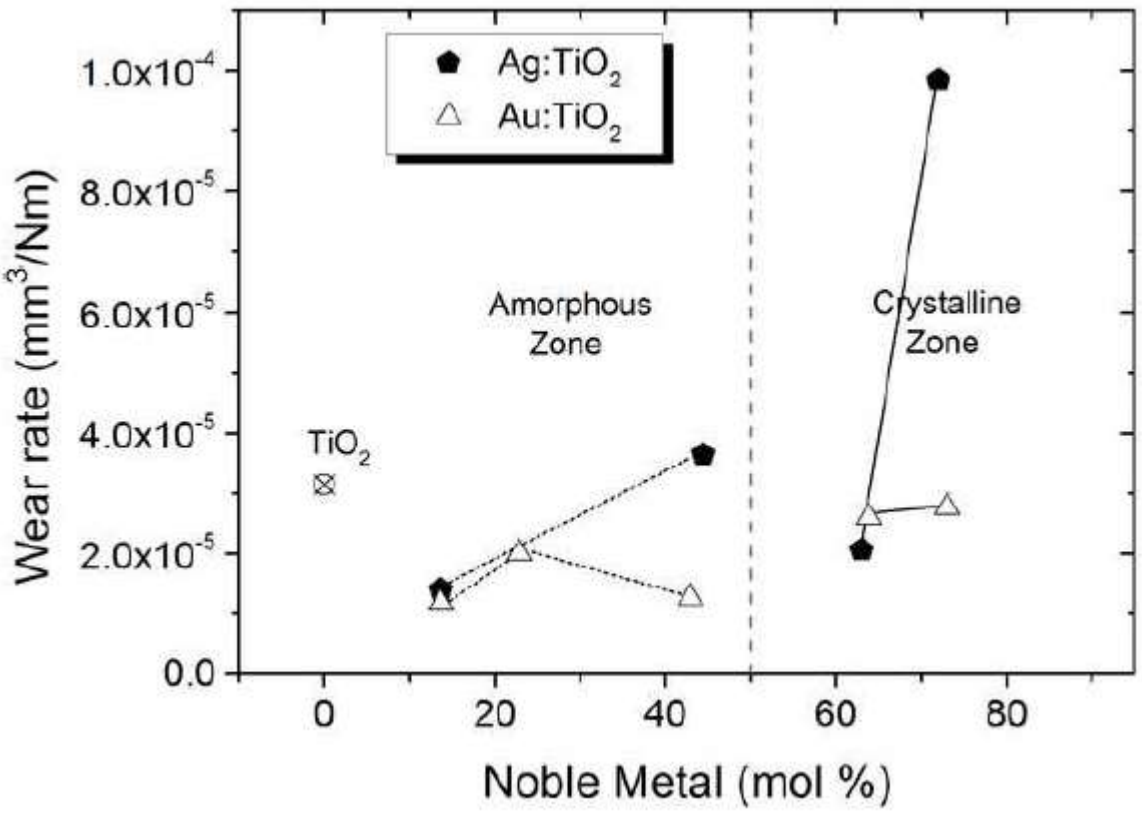
Ag:TiO2
Au:TiO2
Amorphous Zone
Crystalline Zone
TiO2
Wear rate (mm3/Nm)
1.0x10-4
8.0x10-5
6.0x10-5
4.0x10-5
2.0x10-5
0.0
0
20
40
60
80
Noble Metal (mol %)

Figure 6